Inorganic Chemistry

Article

pubs.acs.org/IC

Synthesis of Unsupported d^1–d^x Oxido-Bridged Heterobimetallic Complexes Containing V^{IV}: A New Direction for Metal-to-Metal Charge Transfer

Xinyuan Wu, Tao Huang, Travis T. Lekich, Roger D. Sommer, and Walter W. Weare*

Department of Chemistry, North Carolina State University, Campus Box 8204, Raleigh, North Carolina 27695-8204, United States

Supporting Information

ABSTRACT: Heterobimetallic complexes composed only of first-row transition metals $[(TMTAA)V^{IV}{=}O{\rightarrow}M^{II}Py_5Me_2](OTf)_2$ (TMTAA = 7,16-dihydro-6,8,15,17-tetramethyldibenzo[*b*,*i*][1,4,8,11]tetraazacyclotetradecine; Py_5Me_2 = 2,6-bis(1,1-bis(2-pyridyl)ethyl)pyridine; M = Mn^{II}, Fe^{II}, Co^{II}, Ni^{II}, Cu^{II}; OTf = trifluoromethanesulfonate) have been synthesized through a dative interaction between a terminal oxido and M^{II} metal centers. This is the first series of $V^{IV}{=}O{\rightarrow}M^{II}$ heterobimetallic complexes containing an unsupported oxido bridge. Among these five complexes, only $V^{IV}{=}O{\rightarrow}Fe^{II}$ (**3b**) has a clear new absorption band upon formation of the dinuclear species (502 nm, ε = 1700 M^{-1} cm^{-1}). This feature is assigned to a metal-to-metal charge transfer (MMCT) transition from V^{IV} to Fe^{II}, which forms a V^{V}—O—Fe^{I} excited state. This assignment is supported by electrochemical data, electronic absorption profiles, and resonance Raman spectroscopy and represents the first report of visible-light induced MMCT in a heterobimetallic oxido-bridged molecule where the electron originates on a d^1 metal center.

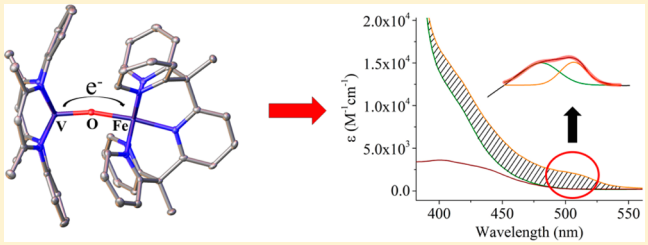

INTRODUCTION

Heterobimetallic oxido-bridged complexes are an important area of transition metal chemistry due to the unique reactivity that can result from the presence of two distinct metal centers.[1] Molecular systems containing a $M_1{-}O{-}M_2$ fragment have been successfully applied as cooperative catalysts for alcohol oxidation,[2] olefin polymerization,[3] and CO_2 reduction.[4−6] Light-driven charge separated excited states induced by intramolecular metal-to-metal charge transfer (MMCT) are also possible, and have been shown in the solid-state to drive photochemical processes such as artificial photosynthesis.[4−14] Redox-active heterobimetallic molecules that contain unsupported oxido bridges are a continued area of interest;[15−17] however, no molecular systems have been definitively shown that possess visible-light induced MMCT transitions.[18] In recent decades a few oxido-bridged complexes containing vanadium have been developed.[19−21] However, structurally characterized mono-oxido-bridged heterobimetallic complexes containing V^{IV} remain rare.[22,23]

Here we report a straightforward synthesis of unsupported oxido-bridged heterobimetallic complexes containing $V^{IV}{=}O{\rightarrow}M^{II}$ (M = Mn, Fe, Co, Ni, and Cu), using (TMTAA)V=O (**1**) (TMTAA = 7,16-dihydro-6,8,15,17-tetramethyldibenzo[*b*,*i*][1,4,8,11]tetraazacyclotetradecine) and $[M^{II}Py_5Me_2](OTf)_2$ (**2a**–**e**) (Py_5Me_2 = 2,6-bis(1,1-bis(2-pyridyl)ethyl)-pyridine) as precursors. These compounds can serve as structural and functional models for photochemically important solid-state MMCT chromophores. The formation of these five new species (**3a**–**e**) has been confirmed by UV−vis, XRD, FTIR, ESI-MS, and cyclic voltammetry. We find that only $V^{IV}{=}O{\rightarrow}Fe^{II}$ (**3b**) has a new, broad feature in the electronic absorption spectra at 490 nm, which is sufficiently described by two Gaussian curves centered at 459 and 502 nm. We have identified that the low-energy portion of this feature is a visible-light induced MMCT transition, where the electron originates from the d^1 vanadium center and is transferred to Fe^{II}, reducing it to Fe^{I} in the excited state. This assignment is supported by electrochemistry and resonance Raman (rRaman) spectroscopy, with only the V→Fe transition being consistent with the observed low-energy excitation. This result is an unusual example of an MMCT transition where the electron transfers from an early to late metal, with all previous studies examining excited states where there is reduction of the early transition metal (such as Ti[14,18] and Zr[4]).

EXPERIMENTAL SECTION

General Considerations. All of the reactions described were carried out in an Innovative Technology glovebox or under an atmosphere of dinitrogen using standard Schlenk techniques. Acetone was dried with $CaSO_4$ and distilled prior to use. Diethyl ether was dried with Na/benzophenone ketyl, distilled, degassed, and stored in the glovebox. Acetonitrile, dichloromethane, toluene, tetrahydrofuran, and pentane were purified using a Grubbs-type, two-column purification system (Innovative Technologies) and stored over 4 Å molecular sieves. All other solvents were purchased from Alfa Aesar and used without further purification. H_2TMTAA,[24] (TMTAA)V=O,[25] Py_5Me_2,[26] metal precursors (for Mn, Fe, and Co),[27] and metal coordinated Py_5Me_2 complexes[28] were synthesized via previously

Received: February 16, 2015
Published: May 13, 2015

DOI: 10.1021/acs.inorgchem.5b00370
Inorg. Chem. 2015, 54, 5322−5328

published synthetic routes. Tetra-*n*-butylammonium hexafluorophosphate (TBAHFP) used for cyclic voltammetry was recrystallized from ethanol and dried under vacuum. Other commercially obtained chemicals were used as received.

Measurements. Electronic absorption spectra (EAS) were recorded using an Olis RSM1000 spectrophotometer with a 1 mm cuvette. ATR-FTIR spectra were obtained on a Bruker Vertex 80 V infrared spectrometer equipped with a Platinum diamond ATR attachment. Electrospray ionization mass spectrometry analyses were carried out on a Thermo Fisher Scientific Exactive Plus MS spectrometer using heated electrospray ionization (HESI) with the compounds dissolved in dichloromethane that had been dried as previously described. Electrochemical data were acquired under anaerobic conditions using a BioLogic S200 potentiostat with glassy carbon as the working electrode, Ag/Ag^+ as the reference electrode, and a Pt wire counter electrode. Cyclic voltammograms were obtained in a nitrogen atmosphere and referenced to added Fc/Fc^+ (0 V) in 0.01 mM TBAHFP dichloromethane solution. Crystal structures were determined by single crystal X-ray diffraction using Bruker-Nonius X8 Kappa Apex II diffractometer with Mo Kα radiation (λ = 0.710 73 Å) at 110(2) K. Crystal structures were solved by direct methods (SHELXS-97) and expanded using difference Fourier techniques. The structures were refined with SHELXL-2013 using full-matrix least-squares calculations.[29] Unless otherwise noted in the Supporting Information, hydrogen atom positions were placed in chemically reasonable positions and refined using geometric constraints using a riding model (U_{iso} of 1.2× or 1.5× parent atom depending on context). H atoms participating in hydrogen bonding were refined freely unless otherwise stated. rRaman spectra were recorded using a custom built system composed of a Princeton Instruments IsoPlane SCT 320 spectrograph and a PIXIS CCD camera with eXcelon technology.[30] Samples were excited using a Coherent Innova 70C Ar/Kr ion laser. Semrock MaxLine laser line filters were utilized to filter the excitations. The rRaman pump was reflected from a 90/10 beam splitter and focused into the sample by a 10× microscope objective. Data was collected at a 180° back scattering geometry. The rRaman signal was collimated by the same objective, and Semrock RazorEdge long pass filters were used to filter the Rayleigh scatter from the rRaman signal in the collection path. The signal was focused into an optical fiber using a 5× microscope objective.

*(TMTAA)V=O (**1**).* This was synthesized using Yang's method,[25] with a modification in the purification conditions. A 15 mL portion of dry toluene was sparged for 20 min with dinitrogen, at which time H_2TMTAA (300 mg, 0.871 mmol), oxidovanadium acetate (180 mg, 0.973 mmol), and triethylamine (88.1 mg, 0.871 mmol) were added. The resulting mixture was heated at reflux for 1 day, during which time a deep green precipitate slowly formed. This crude product was filtered out, washed 3 times with 3 mL of dry toluene, and dried under vacuum. Column chromatography with neutral alumina (50–200 mesh) was used to obtain the pure **1**, washing with dichloromethane to remove unreacted ligand followed by tetrahydrofuran to elute the product as a green band. After the solvent was removed in vacuo, the solid was further dried under vacuum at 80 °C for 3 h. Typical yields for **1** are 30% (107 mg). UV–vis (dichloromethane), λ_{max} (nm) (ε (M^{-1} cm^{-1})): 308 (17 800), 375 (45 500), 416 (10 200). ATR-FTIR: $\nu_{V=O}$ (cm^{-1}): 971. HR ESIMS (M+) m/z calcd for $C_{22}H_{24}N_4OV$ 409.1228, found 409.1224. Anal. Calcd for $C_{22}H_{24}N_4OV$: C, 64.55; H, 5.42; N, 13.68. Found: C, 65.61; H, 5.55; N, 13.92.

*[M^{II}(Py_5Me_2)](CF_3SO_3)$_2$ (**2a–2e**).* Sun's work on [Co(H_2O)-(Py_5Me_2)](CF_3SO_3)$_2$ was applied and extended to the other four metals with minor modifications.[28] Equal molar quantities (0.450 mmol) of metal precursor (**2a**, Mn(CF_3SO_3)$_2$(CH_3CN)$_2$; **2b**, Fe(CF_3SO_3)$_2$(CH_3CN)$_2$; **2d**, Ni(CF_3SO_3)$_2$; **2e**, Cu(CF_3SO_3)$_2$) were combined with Py_5Me_2 in 10 mL of anhydrous acetone. The mixture was stirred at 20 °C for 12 h. After removing the solvent under vacuum, the resulting solid was washed with a minimum amount of acetone and dried under reduced pressure. The products were used without further purification.

*[(TMTAA)V=O→Mn(Py_5Me_2)](CF_3SO_3)$_2$ (**3a**).* Equimolar quantities of **1** (70 mg, 0.171 mmol) and **2a** (136 mg, 0.171 mmol) were added to 6 mL of toluene. The mixture was stirred at 100 °C for 12 h, during which time the mixture slowly turned brown in color. The product was collected over a fritted funnel after being cooled to room temperature, and then washed with minimum amount of toluene and dried under reduced pressure resulting in a light brown solid. Crystals suitable for X-ray diffraction were obtained by slow diffusion of diethyl ether into a dichloromethane solution of **3a**. Yield: 158 mg, 77%. UV–vis (dichloromethane), λ_{max} (nm) (ε (M^{-1} cm^{-1})): 308 (17 000), 375 (44 600), 418 (9700). ATR-FTIR: $\nu_{V=O}$ (cm^{-1}): 901. HR ESIMS (M+) m/z calcd for $[C_{51}H_{47}MnN_9OV]^{2+}$ 453.636, found 453.635. Anal. Calcd for $C_{53}H_{47}F_6MnN_9O_7S_2V{\cdot}C_3H_6O$: C, 53.22; H, 4.23; N, 9.97. Found: C, 53.29; H, 4.20; N, 10.09.

*[(TMTAA)V=O→Fe(Py_5Me_2)](CF_3SO_3)$_2$ (**3b**).* This was synthesized via a similar approach as **3a** using **1** (70 mg, 0.171 mmol) and **2b** (136 mg, 0.171 mmol) in 6 mL of dry toluene, forming an orange-brown solid. Crystals suitable for X-ray diffraction were obtained by slow diffusion of diethyl ether into a dichloromethane solution of **3b**. Yield: 167 mg, 81%. UV–vis (dichloromethane), λ_{max} (nm) (ε ($M^{-1}cm^{-1}$)): 307 (17 700), 375 (41 200), 417 (13 200), 502 (1700). ATR-FTIR: $\nu_{V=O}$ (cm^{-1}): 903. HR ESIMS (M+) m/z calcd for $[C_{51}H_{47}FeN_9OV]^{2+}$ 454.1352, found 454.1343. Anal. Calcd for $C_{53}H_{47}F_6FeN_9O_7S_2V{\cdot}H_2O$: C, 51.98; H, 4.03; N, 10.29. Found: C, 52.03; H, 4.19; N, 10.35.

*[(TMTAA)V=O→Co(Py_5Me_2)](CF_3SO_3)$_2$ (**3c**).* This was synthesized via a similar approach as **3a** using **1** (70 mg, 0.171 mmol) and **2c** (140 mg, 0.171 mmol) in 6 mL of dry toluene, forming a light brown solid. Crystals suitable for X-ray diffraction were obtained by slow diffusion of diethyl ether into a dichloromethane solution of **3c**. Yield: 153 mg, 74%. UV–vis (dichloromethane), λ_{max} (nm) (ε (M^{-1} cm^{-1})): 308 (18 100), 375 (43 000), 419 (9500). ATR-FTIR: $\nu_{V=O}$ (cm^{-1}): 914. HR ESIMS (M+) m/z calcd for $[C_{51}H_{47}CoN_9OV]^{2+}$ 455.6343, found 455.6331. Anal. Calcd for $C_{53}H_{47}F_6CoN_9O_7S_2V{\cdot}H_2O$: C, 51.85; H, 4.02; N, 10.26. Found: C, 51.22; H, 4.17; N, 10.27.

*[(TMTAA)V=O→Ni(Py_5Me_2)](CF_3SO_3)$_2$ (**3d**).* This was synthesized via a similar approach as **3a** using **1** (70 mg, 0.171 mmol) and **2d** (137 mg, 0.171 mmol) in 6 mL of dry toluene forming a greenish brown solid. Crystals suitable for X-ray diffraction were obtained by slow diffusion of diethyl ether into a dichloromethane solution of **3d**. Yield: 153 mg, 74%. UV–vis (dichloromethane), λ_{max} (nm) (ε (M^{-1} cm^{-1})): 306 (17 100), 375 (45 400), 419 (9600). ATR-FTIR: $\nu_{V=O}$ (cm^{-1}): 931. HR ESIMS (M+) m/z calcd for $[C_{51}H_{47}NiN_9OV]^{2+}$ 455.1343, found 455.1341. Anal. Calcd for $C_{53}H_{47}F_6NiN_9O_7S_2V{\cdot}H_2O$: C, 51.86; H, 4.02; N, 10.27. Found: C, 51.17; H, 4.05; N, 10.22.

*[(TMTAA)V=O→Cu(Py_5Me_2)](CF_3SO_3)$_2$ (**3e**).* This was synthesized via a similar approach as **3a** using **1** (70 mg, 0.171 mmol) and **2e** (138 mg, 0.171 mmol) in 6 mL of dry toluene forming a greenish brown solid. Crystals suitable for X-ray diffraction were obtained by slow diffusion of diethyl ether into a dichloromethane solution of **3e**. Yield: 162 mg, 78%. UV–vis (dichloromethane), λ_{max} (nm) (ε (M^{-1} cm^{-1})): 306 (19 000), 376 (46 500), 414 (10 500). ATR-FTIR: $\nu_{V=O}$ (cm^{-1}): 921. Anal. Calcd for $C_{53}H_{47}F_6CuN_9O_7S_2V$: C, 52.42; H, 3.90; N, 10.38. Found: C, 51.19; H, 3.94; N, 9.98.

RESULTS AND DISCUSSION

Synthesis of V^{IV}=O→M^{II} Complexes. Goedken and coworkers have previously reported that **1** can act as a Lewis base to coordinate oxophilic Lewis acids such as $B(C_6H_5)_3$ and $Si(CH_3)_3$.[25] Here, **1** is used similarly, reacting with Lewis acidic first-row transition metals to form heterobimetallic coordination complexes. The Lewis acidic metals are supported by the Py_5Me_2 ligand, which has been shown to accommodate metals of different atomic sizes in stable 2+ oxidation states[31] and is electrochemically silent over a wide potential range.[28,32] These properties make it an excellent ligand environment for studying heterobimetallic photophysics. Moreover, the Py_5Me_2 ligand has only one vacant site available for coordination by a Lewis base, preventing the formation of polymetallic species.[33] Metalation of H_2TMTAA with oxidovanadium acetate and

DOI: 10.1021/acs.inorgchem.5b00370
Inorg. Chem. 2015, 54, 5322–5328

Scheme 1. Formation of Heterobimetallic Complexes 3a−e[a]

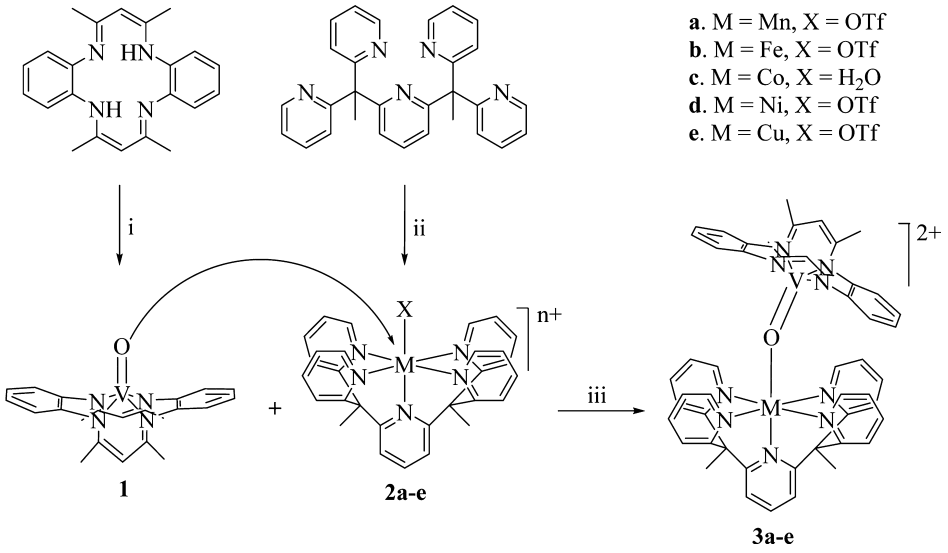

[a] For complexes **2**, n = 1 for **2a**, **2b**, **2d**, **2e** and n = 2 for **2c**. For **3e**, Cu^{II} is five coordinate, with only four of the pyridyl groups of the Py_5Me_2 ligand binding to Cu, which is not schematically shown. Conditions: (i) oxidovanadium acetate, triethylamine, 24 h reflux in toluene; (ii) corresponding metal precursor in acetone at room temperature; (iii) 12 h reflux in toluene.

Py_5Me_2 ligand with the corresponding M^{II} precursor results in complexes **1** and **2a−e**. We have found that careful purification of **1** using a neutral alumina column is necessary for successful, subsequent heterobimetallic formation. Combining equal molar ratios of **1** and **2** in refluxing toluene for 12 h gives the corresponding heterobimetallic products **3** as the only isolable product in good yields (~80%), Scheme 1.

ESI-MS was performed in dichloromethane solution as summarized in the Experimental Section. Complexes **3a−d** clearly show their molecular-ion peak corresponding to $[(TMTAA)V^{IV}{=}O{\rightarrow}M^{II}(Py_5Me_2)]^{2+}$ species, demonstrating their stability in solution. In contrast, **3e** only displays the two mononuclear complexes, suggesting that the $O{\rightarrow}Cu^{II}$ dative bond does not survive under ESI-MS conditions. However, the observation of a 60 cm^{-1} red shift of the signature $\upsilon_{V=O}$ in **3e** is observed by ATR-FTIR, which in combination with the X-ray crystal structure and EA clearly indicates the formation of the heterobimetallic linkage (Table 1, see Supporting Information for complete spectra). This red shift, which is present in all heterobimetallic complexes, is due to coordination of the M^{II} center to the oxygen via a dative interaction; an example of this shift can be seen in Supporting Information Figure S23. This weakens the vanadium oxido bond. Similar behavior is observed in oxido-bridged systems containing $V^{IV}{=}O$[25] and $Ti^{IV}{=}O$.[34,35]

Table 1. $\upsilon_{V=O}$ for Complexes 1 and 3a−e

Complex	$\upsilon_{V=O}$ (cm^{-1})
1 ($V{=}O$)[25]	971
3a ($V{=}O{\rightarrow}Mn$)	901
3b ($V{=}O{\rightarrow}Fe$)	903
3c ($V{=}O{\rightarrow}Co$)	914
3d ($V{=}O{\rightarrow}Ni$)	931
3e ($V{=}O{\rightarrow}Cu$)	921

Crystal Structures. Crystalline materials of sufficient quality for XRD were prepared by vapor diffusion of diethyl ether into dichloromethane solutions. The structures of **1** and **3a−e** were determined by single crystal X-ray diffraction measurements. Two examples (**3a** and **3e**) are shown in Figure 1. Selected parameters are summarized in Table 2. Structures for **3b−d** and detailed unit cell information for **1** and **3a−e** are provided in the Supporting Information.

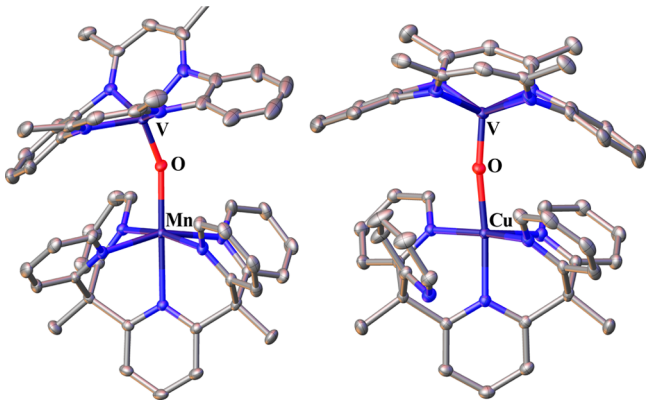

Figure 1. Crystal structures of complex **3a** (left) and **3e** (right) with thermal ellipsoids drawn at the 50% level. Hydrogen atoms and counterions have been omitted for clarity.

This structural data allows for an understanding of unsupported oxido-bridged heterobimetallic $V^{IV}{=}O{\rightarrow}M^{II}$ complexes. **3a** crystallizes in the space group $P\bar{1}$ with two molecules present per unit cell, whereas **3b−d** are monoclinic $P2_1/n$ with four molecules present per unit cell. Structurally, **3a−d** display a similar bonding pattern, with the coordination geometry around vanadium being a distorted square-based pyramid ($N{-}V^{IV}{-}O$ around 110°) and the M^{II} center maintaining a pseudo-octahedral geometry ($N(eq){-}M^{II}{-}O$ ~90°, Figure 1 and Table 2). In **3e**, Cu^{II} is five coordinate, forming a nearly square-based pyramidal geometry (τ = 0.083)[36] with one of the pyridyl arms of Py_5Me_2 remaining uncoordinated (Figure 1). This is due to significant Jahn−Teller distortion, as expected for a d^9 Cu^{II} center, in spite of the

DOI: 10.1021/acs.inorgchem.5b00370
Inorg. Chem. 2015, 54, 5322−5328

Table 2. Selected Structural Parameters of 1 and 3a−e

	1	3a	3b	3c	3d	3e
			Distances (Å)			
V^{IV}−O	1.6090(9)	1.6578(12)	1.6571(19)	1.6475(18)	1.6438(16)	1.6513(12)
V^{IV}−N av	2.0168(11)	2.0087(17)	2.009(2)	2.005(2)	2.0086(19)	2.0006(15)
M^{II}−O	n/a	2.0870(12)	1.9457(19)	2.0244(18)	2.0344(16)	1.9528(12)
M^{II}−N av	n/a	2.2326(15)	1.993(2)	2.123(2)	2.0862(19)	2.0411(14)
V^{IV}−M^{II}	n/a	3.6644(4)	3.5810(6)	3.6523(6)	3.6584(5)	3.5922(4)
			Angles (deg)			
V^{IV}−O−M^{II}	n/a	156.04(8)	167.37(12)	168.09(11)	168.02(10)	170.67(8)
N−V^{IV}−O av	109.79(5)	109.87(6)	109.75(10)	109.37(9)	109.45(8)	109.41(6)
N(eq)−M^{II}−O av	n/a	97.36(5)	90.44(9)	92.97(8)	91.65(7)	94.01(5)
N(ax)−M^{II}−O	n/a	178.21(5)	173.87(9)	172.95(8)	172.91(7)	171.38(5)

highly rigid ligand environment.[26,37] This effect also leads to the observed shorter M—O bond length in **3e** when compared to that in **3a**, with the lower coordination number of **3e** leading to a shorter M—O bond.[38] In the case of **3b**, the shorter bond lengths around Fe^{II} are consistent with a low-spin configuration. The influence of spin state has been observed for similar monometallic complexes using the Py_5 ligand architecture, with significantly shorter bond lengths being observed when antibonding orbitals are not occupied, such as in d^6, low-spin Fe^{II}.[31,39]

The V=O bond lengths for **3a−e** increase by ∼0.04 Å after formation of the dinuclear complexes, which is consistent with the observed decrease of $\upsilon_{V=O}$ by FTIR. The M^{II}—O distances (∼2.00 Å) are significantly longer than V^{IV}=O (∼1.65 Å), which leads us to conclude that the structure is best defined as V^{IV}=O→M^{II}.[20,21] The V^{IV}—M^{II} distances vary from 3.58 to 3.66 Å depending on the M^{II} center. **3a−e** each shows a slightly bent structure for the oxido bridge, with the V^{IV}—O—M^{II} angle in a range 156−170°. This is consistent with other heterobimetallic oxido-bridged systems containing vanadium.[20,21,25]

Electrochemistry. In order to probe the electrochemical behavior of these new heterobimetallic systems, cyclic voltammetric measurements were performed on mononuclear **1**, **2a−e**, and binuclear **3a−e** (see Supporting Information Figures S39 and S40). The vanadium precursor, **1**, has a single quasireversible oxidative redox event at −0.22 V (vs Fc/Fc^+ = 0 V as for all other potentials; Fc = ferrocene), which was previously assigned as $V^{V/IV}$.[40] An irreversible oxidation at 1.27 V is assigned to ligand oxidation processes, and is in agreement with a previous assignment from the related titanium complex (TMTAA)Ti=O.[34] As summarized in Table 3, complexes **2a−e** demonstrate metal-based one-electron oxidative and reductive redox waves. The quasireversible $Mn^{III/II}$, $Fe^{III/II}$, $Co^{III/II}$, $Ni^{III/II}$ oxidative couples are observed at 0.76, 0.83, 0.44, and 1.42 V, respectively, while the irreversible reductive $Fe^{II/I}$, $Co^{II/I}$, $Ni^{II/I}$ couples are identified at −2.09, −1.52, and −1.73 V. Compound **2e** has only one quasireversible wave at −0.36 V, corresponding to $Cu^{II/I}$.

The electrochemical behavior of binuclear complexes **3a−e** are depicted in Supporting Information Figure S40, and their featured redox couples are summarized in Table 3. The binuclear complex **3e** has two quasireversible redox processes that are assigned to $Cu^{II/I}$ and $V^{V/IV}$, respectively. When compared to the mononuclear (TMTAA)V=O species, the $V^{V/IV}$ redox couple is anodically shifted from −0.22 to −0.15 V and $Cu^{II/I}$ redox couple shifts anodically from −0.36 to −0.22 V. For complexes **3a−d**, the redox behavior is classified into four voltage regions (Figure 2) for comparison purposes. Process I is an irreversible reductive event that happens at potential between −1.97 and −1.55 V. Since these redox waves are at the similar range as $M^{II/I}$ (M = Mn, Fe, Co, Ni) redox couples of **2a−d**, they have been assigned as $Mn^{II/I}$ (−1.99 V), $Fe^{II/I}$ (−1.97 V), $Co^{II/I}$ (−1.55 V), and $Ni^{II/I}$ (−1.75 V), respectively. Process II is in the range between −0.20 and 0.20 V, which is assigned as $V^{V/IV}$. Compound **3b** has two distinguishable electrochemical responses within this range.

Table 3. Summary of Electrochemical Potentials of Complexes 1, 2a−e, and 3a−e[a]

complex	$M^{II/I}$ (E_{pc}/V)	$V^{V/IV}$ ($E_{1/2}$/V)	$M^{III/II}$ ($E_{1/2}$/V)	L oxidation (V)
1		−0.22		1.27[b]
2a			0.76	
2b	−2.09[b]		0.83	
2c	−1.52[b]		0.44	
2d	−1.73[b]		1.42	
2e	−0.36			
3a	−1.99[b]	−0.15	0.81	
3b	−1.97[b]	0.13[c]	0.64	1.21[b]
3c	−1.55[b]	−0.18	0.41	1.26[b]
3d	−1.75[b]	−0.17	1.44	1.25[b]
3e	−0.22	−0.15		

[a]All values are referenced vs Fc/Fc^+ = 0 V. [b]Denotes an irreversible transition. [c]Determined by variable-rate voltammetry.

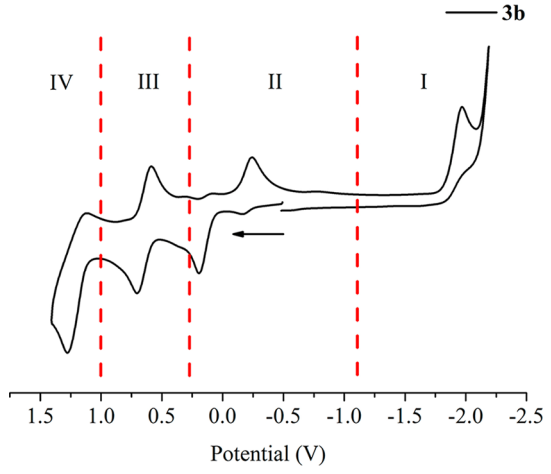

Figure 2. Cyclic voltammogram of **3b**, with four redox regions labeled. Fc/Fc^+ = 0 V which was added after this voltammogram was recorded as an internal standard.

DOI: 10.1021/acs.inorgchem.5b00370
Inorg. Chem. 2015, 54, 5322−5328

The first redox wave at approximately −0.20 V is assigned to $V^{V/IV}$ of **1**, a result of the dissociation of the complex to form the mononuclear (TMTAA)V=O under electrochemical conditions. The second redox wave at ∼0.13 V is assigned to $V^{V/IV}$ in intact **3b** (Figure 2), and is significantly shifted (∼0.35 V) compared to **1**. The $V^{V/IV}$ couple for **3a** and **3c**−**e** do not shift significantly upon heterobimetallic formation. This assignment for **3b** is supported by a variable scan rate study (Supporting Information Figure S41), with the reported $E_{1/2}$ value for $Fe^{II/I}$ being determined using this experiment. As the scan rate increases, the wave at 0.20 V (assigned to **3b**) changes from irreversible to quasireversible; by controlling the range of scan potential, the intensity of the reduction wave at −0.20 V (assigned to **1**) increases after the potential passes the region of V^{IV} oxidation in **3b**. This phenomenon is consistent with slow dissociation in solution under the electrochemical conditions. Similar dissociation reactions are also observed in Ti=O→Cr systems.[34] Process III is assigned to the range 0.44−1.44 V, which is attributed to $M^{III/II}$ (M = Mn, Fe, Co, Ni). The redox couples of $Mn^{III/II}$ (0.81 V), $Co^{III/II}$ (0.41 V), and $Ni^{III/II}$ (1.44 V) undergo only minor shifts upon formation of the binuclear complexes (**3a** = 0.76 V, **3c** = 0.44 V, and **3d** = 1.42 V, respectively), consistent with the absence of substantial shifts in $V^{V/IV}$. In contrast, $Fe^{III/II}$ cathodically shifts by 0.19 V upon formation of the bimetallic **3b** (**2b** = 0.83 V and **3b** = 0.64 V), which when combined with the observation of $V^{V/IV}$ in **3b** indicates the presence of an interaction between V^{IV} and Fe^{II} that is not present in the other heterobimetallic complexes. Process IV is due to ligand oxidation events which normally lie at ∼1.26 V, and undergo only minor shifts from **1** upon formation of the bimetallic species. Overall, the electrochemical data shows that small, but tangible changes occur for the $V^{V/IV}$, $M^{II/I}$, and $M^{III/II}$ in all systems other than **3b**. In **3b** significant changes in the redox behavior of both metal centers occur upon formation of the bimetallic species. In the absence of water or oxygen, solutions of **3a**−**e** did not undergo any changes in their absorption features or electrochemical responses even after several weeks in solution.

MMCT in V^{IV}=O→Fe^{II} System. Electronic absorption spectra were measured for **3a**−**e** to probe the electronic transitions of these heterobimetallic systems. For **3a**, **3c**, **3d**, and **3e**, the absorption profiles are nearly indistinguishable from the **1** (see Supporting Information for full spectrum), with minor changes in molar absorptivity observed due to the changes in symmetry upon formation of heterobimetallic species. In contrast, the spectrum of V^{IV}=O→Fe^{II} complex **3b** shows significant differences when compared with the two starting mononuclear complexes (Figure 3). In particular a new broad absorption is observed which extends from 400 to 550 nm, roughly centered at 490 nm.

In order to elucidate this new feature, a mathematic difference spectrum (**3b** − **2b** − **1**) was computed (Figure 4). This method has been previously utilized to assign new electronic transitions due to MMCT.[11,12,14,18] The negative components at energies higher than 3.00 eV correspond to intensity losses in the mononuclear-based (TMTAA)V=O transitions. The positive region between 3.00 and 2.10 eV indicates new electronic transitions upon formation of **3b**. This new feature could be adequately fit by two Gaussian peaks centered at 2.70 eV (459 nm) and 2.47 eV (502 nm). The 2.70 eV (459 nm) peak is assigned to a red-shifted ligand-to-metal charge transfer (LMCT) at vanadium, and is consistent with the observed anodic shift of $V^{V/IV}$. The peak at 2.47 eV (502 nm) is assigned to a new MMCT transition from V^{IV} to Fe^{II}, forming a charge separated excited state composed of V^{V} and Fe^{I}. To make this assignment, we examined the electrochemistry of **3b** and found that only the $V^{V/IV}$ and $Fe^{II/I}$ redox couples have a plausible energy gap to explain this transition (ΔE = 2.10 V). This provides a good match for the 2.47 eV band. All alternative assignments result in energies that are larger than 2.5 eV. The most likely alternative assignment, an MMCT from Fe^{II} to V^{IV}, would involve $V^{IV/III}$, which is not observed throughout the solvent window (∼−1.5 V). This means that the energy difference between $V^{IV/III}$ and $Fe^{III/II}$ can be no smaller than 2.90 eV, and therefore cannot explain the observed absorption features.

To further support our assignments, rRaman spectra of **3b** was mapped at three different wavelengths throughout the new transitions.[22,41−43] Normalized rRaman spectra are shown in Figure 5, with a superimposition of difference spectra and the relative rRaman intensity of $\upsilon_{V=O}$ (Figure 6). A significant enhancement is observed at 910 cm^{-1}, which corresponds to $\upsilon_{V=O}$ as observed by FTIR (see ref 22 and Table 1).

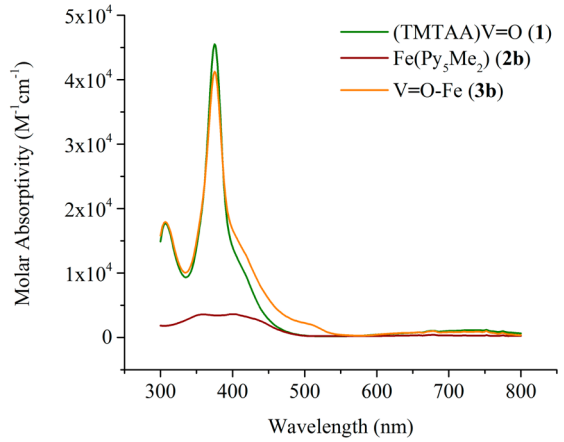

Figure 3. Electronic absorption spectra of **1**, **2b**, and **3b**. A new, broad absorption feature is observed that is approximately centered at 490 nm.

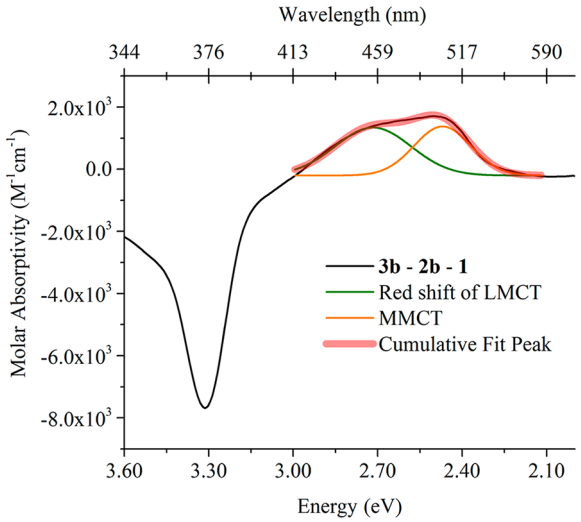

Figure 4. Electronic absorption difference spectrum resulting from subtracting the sum of **1** and **2b** from the spectrum of heterobimetallic **3b**. The result was fit to a combination of two Gaussian peaks centered at 2.70 eV (green) and 2.47 eV (orange).

DOI: 10.1021/acs.inorgchem.5b00370
Inorg. Chem. 2015, 54, 5322−5328

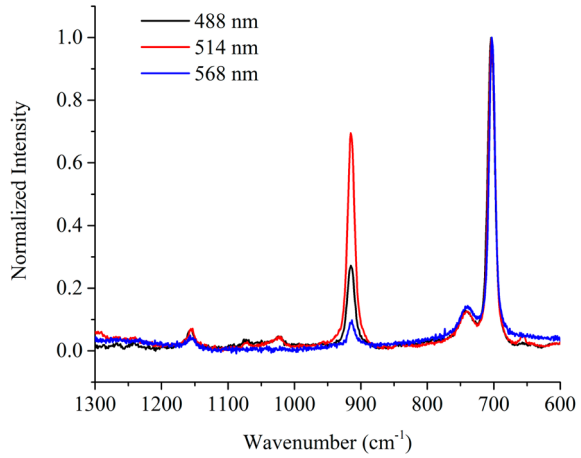

Figure 5. Normalized resonance Raman spectra of **3b** in dichloromethane. Black, 488 nm excitation; red, 514 nm excitation; blue, 568 nm excitation. Wavelength and intensity were referenced and normalized to the rRaman signal of dichloromethane (703 cm^{-1}).

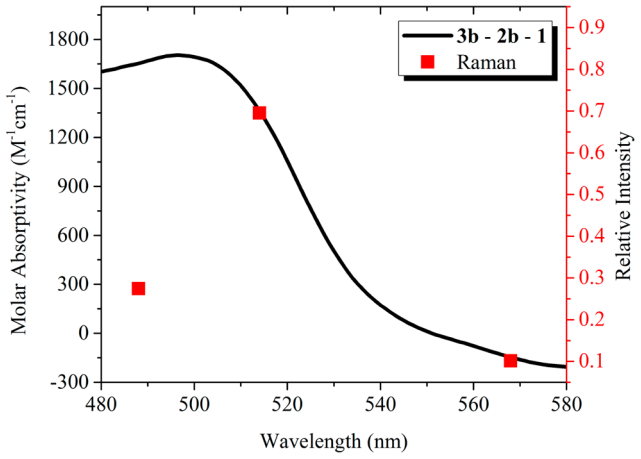

Figure 6. Resonance Raman enhancement profile (■) overlaid with the difference spectra (**3b** − **2b** − **1**, solid curve). Plotted rRaman intensities $\upsilon_{V=O}$ (910 cm^{-1}) are relative to the solvent reference peak and intensity matched to the difference spectrum at 516 nm, showing that only the low-energy band is associated with the oxido bridge distortion.

This enhancement would only be possible for a transition where the structural distortions during excited state electron transfer coincide with vibrations localized on the bridge. Of the two assignments (LMCT and MMCT), only a MMCT transition (502 nm) would result in distortions coupled to the bridge modes. Since only excitation in the low-energy portion of the new absorption results in resonant enhancement, this result supports our assignment that the lower energy transition is due to MMCT. The higher energy band (459 nm) appears to not contribute to this feature and therefore cannot involve transitions that distort the V−O−Fe bond, supporting our assignment of this transition as being due to LMCT from the TMTAA ligand. No rRaman enhancement at 910 cm^{-1} is observed for either of the mononuclear components (**1** or **2b**) when excited in this range (Supporting Information Figure S43). The small (8 cm^{-1}) difference $\upsilon_{V=O}$ between the FTIR and rRaman spectra is a result of FTIR being a solid-state measurement while rRaman was measured in a saturated dichloromethane solution.

The observation that only **3b** has new transitions ultimately raises the question of why is the V=O→Fe complex different from the other species? Upon examination of the crystal structures, only **3b** is found to be low-spin. As a result, **3b** is the only complex in the series that definitively has an unoccupied σ^* orbital (d^6 low-spin). We therefore speculate that such unoccupied orbitals are necessary for the observation of MMCT transitions in these oxido-bridged heterobimetallic molecules, potentially acting as the orbital into which the electron transfer occurs.

CONCLUSION

Five new heterobimetallic oxido-bridged complexes containing d^1 vanadium have been synthesized and structurally confirmed. All five species are formed through a dative interaction between the oxido and a M^{II} metal center, with a slightly bent V=O—M angle varying from 156° to 170°. A Jahn−Teller distortion was observed in the Cu center of V=O→Cu, resulting in five coordinate Cu^{II}. Cyclic voltammetry reveals clear $V^{V/IV}$, $M^{II/I}$, and $M^{III/II}$ redox couples in four voltage regions. Surprisingly, only the V=O→Fe system is found to have a strong interaction between the two metal centers, with a significant shift of redox potentials on both sides of the oxido bridge and the appearance of a new optical transition in the visible region (502 nm, ε = 1700 M^{-1} cm^{-1}) which we assign to a V^{IV} to Fe^{II} MMCT. This assignment is supported by rRaman spectroscopy, which shows that this transition is associated with vibrational modes from the oxido bridge. We speculate that the presence of an MMCT transition in the Fe^{II} complex is due to the presence of empty σ^* orbitals in this low-spin d^6 complex. To our knowledge, this is the first observation of a MMCT transition from a d^1 metal center, opening up a new direction for the study of visible-light induced MMCT.

ASSOCIATED CONTENT

Supporting Information

Electronic absorption spectra, ATR-FTIR spectra, HRMS results, crystallographic details, electrochemical measurements, and resonance Raman experiments. Crystallographic data in CIF format. The Supporting Information is available free of charge on the ACS Publications website at DOI: 10.1021/acs.inorgchem.5b00370.

AUTHOR INFORMATION

Corresponding Author

*E-mail: wwweare@ncsu.edu.

Notes

The authors declare no competing financial interest.

ACKNOWLEDGMENTS

The authors acknowledge financial support from the North Carolina State University Department of Chemistry. We thank Michelle McGoorty, Dr. Evgeny Danilov, and Prof. Felix Castellano for assistance with resonance Raman spectroscopy. Mass spectra were obtained at the NCSU Department of Chemistry Mass Spectrometry Facility.

REFERENCES

(1) West, B. O. *Polyhedron* **1989**, *8*, 219−247.
(2) Shapley, P. A.; Zhang, N. J.; Allen, J. L.; Pool, D. H.; Liang, H. C. *J. Am. Chem. Soc.* **2000**, *122*, 1079−1091.

DOI: 10.1021/acs.inorgchem.5b00370
Inorg. Chem. 2015, 54, 5322−5328

(3) Gurubasavaraj, P. M.; Roesky, H. W.; Sharma, P. M. V.; Oswald, R. B.; Dolle, V.; Herbst-Irmer, R.; Pal, A. *Organometallics* **2007**, *26*, 3346−3351.
(4) Kim, W.; Yuan, G.; McClure, B. A.; Frei, H. *J. Am. Chem. Soc.* **2014**, *136*, 11034−11042.
(5) Lin, W.; Frei, H. *J. Am. Chem. Soc.* **2005**, *127*, 1610−1611.
(6) Lin, W.; Frei, H. *C. R. Chim.* **2006**, *9*, 207−213.
(7) Wu, X.; Weare, W. W.; Frei, H. *Dalton Trans.* **2009**, 10114−10121.
(8) Cuk, T.; Weare, W. W.; Frei, H. *J. Phys. Chem. C* **2010**, *114*, 9167−9172.
(9) Takashima, T.; Yamaguchi, A.; Hashimoto, K.; Nakamura, R. *Chem. Commun.* **2012**, *48*, 2964−2966.
(10) Okamoto, A.; Nakamura, R.; Osawa, H.; Hashimoto, K. *J. Phys. Chem. C* **2008**, *112*, 19777−19783.
(11) Han, H. X.; Frei, H. *Microporous Mesoporous Mater.* **2007**, *103*, 265−272.
(12) Han, H. X.; Frei, H. *J. Phys. Chem. C* **2008**, *112*, 8391−8399.
(13) Soo, H. S.; Macnaughtan, M. L.; Weare, W. W.; Yano, J.; Frei, H. *J. Phys. Chem. C* **2011**, *115*, 24893−24905.
(14) McClure, B. A.; Frei, H. *J. Phys. Chem. C* **2014**, *118*, 11601−11611.
(15) Nichols, P. J.; Fallon, G. D.; Moubaraki, B.; Murray, K. S.; West, B. O. *Polyhedron* **1993**, *12*, 2205−2213.
(16) Chufan, E. E.; Verani, C. N.; Puiu, S. C.; Rentschler, E.; Schatzschneider, U.; Incarvito, C.; Rheingold, A. L.; Karlin, K. D. *Inorg. Chem.* **2007**, *46*, 3017−3026.
(17) Vernik, I.; Stynes, D. V. *Inorg. Chem.* **1998**, *37*, 10−17.
(18) Falzone, A. J.; Nguyen, J.; Weare, W. W.; Sommer, R. D.; Boyle, P. D. *Chem. Commun.* **2014**, *50*, 2139−2141.
(19) Wanandi, P. W.; Davis, W. M.; Cummins, C. C.; Russell, M. A.; Wilcox, D. E. *J. Am. Chem. Soc.* **1995**, *117*, 2110−2111.
(20) Bhattacharya, K.; Maity, M.; Mondal, D.; Endo, A.; Chaudhury, M. *Inorg. Chem.* **2012**, *51*, 7454−7456.
(21) Bhattacharya, K.; Abtab, S. M.; Majee, M. C.; Endo, A.; Chaudhury, M. *Inorg. Chem.* **2014**, *53*, 8287−8297.
(22) Dean, N. S.; Cooper, J. K.; Czernuszewicz, R. S.; Ji, D.; Carrano, C. J. *Inorg. Chem.* **1997**, *36*, 2760−2764.
(23) Mohanta, S.; Nanda, K. K.; Thompson, L. K.; Flörke, U.; Nag, K. *Inorg. Chem.* **1998**, *37*, 1465−1472.
(24) Goedken, V. L.; Weiss, M. C.; Place, D.; Dabrowiak, J. *Inorg. Synth.* **1980**, *20*, 115−119.
(25) Yang, C. H.; Ladd, J. A.; Goedken, V. L. *J. Coord. Chem.* **1988**, *18*, 317−334.
(26) Bechlars, B.; D'Alessandro, D. M.; Jenkins, D. M.; Iavarone, A. T.; Glover, S. D.; Kubiak, C. P.; Long, J. R. *Nat. Chem.* **2010**, *2*, 362−368.
(27) Dixon, N. E.; Lawrance, G. A.; Lay, P. A.; Sargeson, A. M.; Taube, H. *Inorg. Synth.* **1990**, *28*, 70−76.
(28) Sun, Y.; Bigi, J. P.; Piro, N. A.; Tang, M. L.; Long, J. R.; Chang, C. J. *J. Am. Chem. Soc.* **2011**, *133*, 9212−9215.
(29) Sheldrick, G. M. *Acta Crystallogr., Sect. A* **2008**, *64*, 112−122.
(30) Stanton, I. N.; Belley, M. D.; Nguyen, G.; Rodrigues, A.; Li, Y.; Kirsch, D. G.; Yoshizumi, T. T.; Therien, M. J. *Nanoscale* **2014**, *6*, 5284−5288.
(31) Gebbink, R. J. M. K.; Jonas, R. T.; Goldsmith, C. R.; Stack, T. D. P. *Inorg. Chem.* **2002**, *41*, 4633−4641.
(32) Karunadasa, H. I.; Chang, C. J.; Long, J. R. *Nature* **2010**, *464*, 1329−1333.
(33) Jeon, I. R.; Calancea, S.; Panja, A.; Piñero Cruz, D. M.; Koumousi, E. S.; Dechambenoit, P.; Coulon, C.; Wattiaux, A.; Rosa, P.; Mathonière, C.; Clérac, R. *Chem. Sci.* **2013**, *4*, 2463−2470.
(34) Huang, T.; Wu, X.; Weare, W. W.; Sommer, R. D. *Eur. J. Inorg. Chem.* **2014**, 5662−5674.
(35) Yang, C. H.; Ladd, J. A.; Goedken, V. L. *J. Coord. Chem.* **1988**, *19*, 235−251.
(36) Addison, A. W.; Rao, T. N.; Reedijk, J.; van Rijn, J.; Verschoor, G. C. *J. Chem. Soc., Dalton Trans.* **1984**, 1349−1356.
(37) Jahn, H. A.; Teller, E. *Proc. R. Soc., Ser. A* **1937**, *161*, 220−235.
(38) Batsanov, S. S. *J. Struct. Chem.* **2010**, *51*, 281−287.
(39) Goldsmith, C. R.; Jonas, R. T.; Cole, A. P.; Stack, T. D. P. *Inorg. Chem.* **2002**, *41*, 4642.
(40) Schumann, H. *Inorg. Chem.* **1996**, *35*, 1808−1813.
(41) San Filippo, J.; Fagan, P. J.; Di Salvo, F. J. *Inorg. Chem.* **1977**, *16*, 1016−1021.
(42) Sanders-Loehr, J.; Wheeler, W. D.; Shiemke, A. K.; Averill, B. A.; Loehr, T. M. *J. Am. Chem. Soc.* **1989**, *111*, 8084−8093.
(43) Inscore, F. E.; McNaughton, R.; Westcott, B. L.; Helton, M. E.; Jones, R.; Dhawan, I. K.; Enemark, J. H.; Kirk, M. L. *Inorg. Chem.* **1999**, *38*, 1401−1410.

DOI: 10.1021/acs.inorgchem.5b00370
Inorg. Chem. 2015, 54, 5322−5328